

Tracking the impact of environment on the Galaxy Stellar Mass Function up to $z \sim 1$ in the 10k zCOSMOS sample ^{*}

M. Bolzonella¹, K. Kovač², L. Pozzetti¹, E. Zucca¹, O. Cucciati³, S. J. Lilly², Y. Peng², A. Iovino⁴, G. Zamorani¹, D. Vergani¹, L. A. M. Tasca^{5,3}, F. Lamareille⁶, P. Oesch², K. Caputi², P. Kampczyk², S. Bardelli¹, C. Maier², U. Abbas⁷, C. Knobel², M. Scodeggio⁵, C. M. Carollo², T. Contini⁶, J.-P. Kneib³, O. Le Fèvre³, V. Mainieri⁸, A. Renzini⁹, A. Bongiorno¹⁰, G. Coppia^{1,11}, S. de la Torre⁴, L. de Ravel³, P. Franzetti⁵, B. Garilli⁵, J.-F. Le Borgne⁶, V. Le Brun³, M. Mignoli¹, R. Pelló⁶, E. Perez-Montero^{6,12}, E. Ricciardelli⁹, J. D. Silverman², M. Tanaka⁸, L. Tresse³, D. Bottini⁵, A. Cappi¹, P. Cassata¹³, A. Cimatti¹¹, L. Guzzo⁴, A. M. Koekemoer¹⁴, A. Leauthaud¹⁵, D. Maccagni⁵, C. Marinoni¹⁶, H. J. McCracken¹⁷, P. Memeo⁵, B. Meneux¹⁰, C. Porciani¹⁸, R. Scaramella¹⁹, H. Aussel²⁰, P. Capak²¹, O. Ilbert³, J. Kartaltepe²², M. Salvato²¹, D. Sanders²², C. Scarlata²³, N. Scoville²¹, Y. Taniguchi²⁴, and D. Thompson²⁵

(Affiliations can be found after the references)

Preprint online version: June 30, 2009

ABSTRACT

We study the impact of the environment on the evolution of galaxies in the zCOSMOS 10k sample in the redshift range $0.1 \leq z \leq 1.0$ over an area of $\sim 1.5 \text{ deg}^2$. The considered sample of secure spectroscopic redshifts contains about 8500 galaxies, with their stellar masses estimated through SED fitting of the multi-wavelength optical to Near-Infrared photometry. The evolution of the Galaxy Stellar Mass Function (GSMF) in high and low density regions provides a tool to study the mass assembly evolution in different environments; moreover, the contributions to the GSMF from different galaxy types, as defined by their SEDs and their morphologies can be quantified. At redshift $z \sim 1$ the GSMF is only slightly dependent on environment, but at lower redshifts the shapes of the GSMFs in high- and low-density environments become extremely different, with high density regions exhibiting a marked bimodality, not reproducible by a single Schechter function. Galaxy evolution depends both on the stellar mass and on the environment, setting the probability of a galaxy to have a given mass. All the galaxy properties related to the stellar mass will show a dependence on the environment, reflecting the difference observed in the mass functions. The shape of the GSMFs of early and late type galaxies is quasi-universal, i.e., it is consistent to be the same in the extreme environments we considered. The evolution toward $z = 0$ of the transition mass M_{cross} , i.e., the mass at which the early and late type GSMFs match each other, is more rapid in high density environments. The same result can be obtained studying the relative contribution of different galaxy types, implying a faster evolution in overdense regions, in particular for intermediate stellar masses. The rate of evolution is different when dividing galaxy types on the basis of their SEDs or their morphologies, tentatively suggesting that the migration from the blue cloud to the red sequence is occurring on a shorter timescale than the transformation from disc-like morphologies to ellipticals. Environmental mechanisms of galaxy transformation are at work at $z < 1$. The comparison of the observed GSMFs to the same quantities derived from a set of mock catalogues based on semi-analytical models shows a disagreement, both in low and high density environments.

Key words. Cosmology: observations – Galaxies: fundamental parameters, mass function, evolution

1. Introduction

The environmental dependence of galaxy properties (colour, star formation, mass) is a well known effect in the local universe. At present many local studies have been carried out to analyse the influence of environment on colours, luminosities, morphologies, structural parameters, star formation and stellar masses: all local relations are somewhat linked to the morphology-density relation shown by Dressler (1980).

At higher redshifts this kind of study becomes very difficult, because the need of large spectroscopic samples of faint galaxies with a good sampling rate hampers a reliable estimate of the environment. Up to now, therefore, most of the high den-

sity environments coincided with galaxy clusters or groups and the more general effect of the environment on field galaxy evolution is still poorly explored. The evolution of the Galaxy Stellar Mass Function (GSMF) as a function of the large scale environment has been studied in the DEEP2 Galaxy Redshift Survey (Bundy et al. 2006), considering the redshift range $z = 0.4 - 1.4$, which limits the connection between this study and those in the local Universe.

Some of the still open question are: which is the leading property in the evolution of field galaxies? Is the fate of a galaxy decided once its mass is defined or do some external players have a role? And, if the environment plays such a role, when does it start to affect galaxy evolution, and through which mechanism?

Looking at literature results, the full picture of the story of galaxies is not unanimous. At low redshifts, Balogh et al. (2001), using 2MASS and LCRS data, separated different environments as field, groups and clusters, finding that Luminosity and Mass Functions depend both on galaxy type (with steeper functions for emission line galaxies) and environment (with more massive

Send offprint requests to: Micol Bolzonella
e-mail: micol.bolzonella@oabo.inaf.it

^{*} Based on observations obtained at the European Southern Observatory(ESO) Very Large Telescope (VLT), Paranal, Chile, as part of the Large Program 175.A-0839 (the zCOSMOS Spectroscopic Redshift Survey).

and brighter objects more common in clusters), mainly as a consequence of the different contribution of passive galaxies.

Most of the low-redshift studies are based on the SDSS data: studying the colour bimodality, Balogh et al. (2004) found that, even if the mean colour of red and blue galaxies depends only marginally on environment, the fraction of red galaxies significantly increases toward high densities at fixed luminosity; they propose that the properties of star forming galaxies are mainly related to their mass and that, to preserve the bimodality without altering the colours modelled by two Gaussian distributions, the transformation from late to early type galaxies should be rapid in truncating the star formation and efficient for all luminosities and environments. In an analogous study, Hogg et al. (2003) reached similar conclusions, with blue galaxies showing no correlation between their luminosity/mass and local density at a fixed colour. In a comprehensive analysis on environmental dependence of galaxy properties in the SDSS, Kauffmann et al. (2004) found evidences supporting a mix of both nature and nurture scenarios, where the star formation history is the galaxy property more dependent on environment. Tanaka et al. (2004) studied the environmental dependence of star formation and morphologies: they pointed out that environment is more effective on faint galaxies, affecting more their star formation and morphology in dense regions above a critical density, whereas the properties of bright galaxies do not show any dependence on environment. Blanton et al. (2005) found that the star formation history and the mass of bright galaxies of the SDSS are more dependent on environment than structural parameters, like the surface brightness and profile shape. Baldry et al. (2006), using a sample limited at $z < 0.1$ and a projected density estimator, found that the characteristic mass contributing the most to the stellar mass density increases with density from $10^{10.6}$ to $10^{10.9} M_{\odot}$ and the fraction of galaxies in the red sequence increases as a function of mass and density: they concluded that both the stellar mass and the environment, which cannot be considered as a second order effect, determine the probability of a galaxy being in the red sequence. Baldry et al. (2008) computed the local estimate of the GSMF detecting a low mass upturn at $\sim 10^9 M_{\odot}$, like the one observed in galaxy clusters, but the dominant galaxy types and the processes producing the bimodality of the GSMFs should be different in clusters and in the field. Mateus et al. (2008) used SDSS data and compared their results to the Millennium simulation: they also supported the nurture-like scenario, with environment playing a fundamental role in defining the galaxy properties and confirmed the findings by Mateus et al. (2007): galaxy evolution takes place in an accelerated way at high redshift in denser environments, where massive galaxies preferentially reside. Following the study by Lee & Li (2008) on SDSS, the initial conditions significantly contribute in establishing the environmental dependence of galaxy properties, even if in the densest regions the initial correlation between galaxy properties and environment will be superseded by non linear processes at small-scales. Recently, van den Bosch et al. (2008) investigated the efficiency of transformation processes, using a group catalogue drawn from the SDSS: the colour and the concentration of a satellite galaxy are almost completely determined by their stellar mass, with only a very mild dependence on environment.

At higher redshifts, probing the effect of environment on galaxy evolution becomes more difficult and often this kind of studies uses projected estimators of local density and relies on photometric redshifts. The main spectroscopic study carried out up to now estimating the effect of environment on GSMFs has been presented by Bundy et al. (2006): using DEEP2 data at

$0.4 < z < 1.4$ and $R_{AB} < 24.1$ they drew the conclusion that the quenching of star formation, and then the transition between the blue cloud and the red sequence, is primarily internally driven and dependent on mass, even if they detected a moderate acceleration of the downsizing phenomenon in overdense regions, where the rise of the quiescent population with cosmic time appears to be faster, as seen through the evolution of the transition and quenching masses, M_{cross} and M_Q .

Using the same dataset complemented by SDSS at low redshifts, Cooper et al. (2008) studied the connection between the Star Formation Rate (SFR) and environment, finding hints for a reversal of that relation from $z \sim 0$, where the mean SFR is decreasing with local density, to $z \sim 1$, where a blue population causes an increase of the mean SFR in overdense regions; nonetheless, the decline of the global cosmic star formation history since $z \sim 1$ seems to be due to a gradual gas consumption rather than environment-dependent processes: the fall of the mean SFH from $z \sim 1$ to $z \sim 0$ is much stronger than its dependence on environment, which can be regarded as a small perturbing effect to the global trend. A similar result on the reversing relationship SFR-environment has been achieved by Elbaz et al. (2007), using GOODS data and SFR derived from UV and $24 \mu\text{m}$ emission. Looking at the evolution of the colour-density relation, Cucciati et al. (2006) used spectroscopic data from the VVDS up to $z \sim 1.5$: they found a steep relation at low- z , tending to disappear at higher redshifts. In particular, they identified differences in colour distributions in low and high density regimes at low redshifts, whereas at high redshifts the environment is not affecting such a distribution. In their proposed scenario the processes of star formation and gas exhaustion are accelerated for more luminous objects and high density environments, leading to a shift with cosmic time of the star formation activity toward fainter galaxies and low density environments. Scodreggio et al. (2009) studied the stellar mass and colour segregations in the VVDS at redshifts $z = 0.2 - 1.4$, using a density field computed on scales of ~ 8 Mpc; they found that the colour-density relation is a mirror of the stellar mass segregation, that in turn is a consequence of the dark matter halo mass segregation predicted by hierarchical models.

Both the effects of environment on local galaxy properties and on their evolution are still uncertain, making the nature vs nurture debate still open. From the aforementioned results, there seems to be some hint that the galaxy evolutionary path from the blue cloud to the red sequence depends on environment, but the determination of the mechanism of such a transformation, its probability, its link to the environment and to the innate galaxy properties is a difficult task. Different physical processes of galaxy transformation will differ on timescales, on efficiency and on the observational repercussions, like colour and morphology. The GSMF is a very suitable tool to investigate this problem and to witness the buildup of galaxies and its dependence on environment.

In this paper we will focus on the effect of environment on field galaxies, avoiding the most extreme overdense regions like cluster cores, and we will use data from COSMOS (Cosmic Evolution Survey) and zCOSMOS; parallel and complementary analyses are presented in Pozzetti et al. (2009), Zucca et al. (2009), Iovino et al. (2009), Cucciati et al. (2009), Tasca et al. (2009), Kovač et al. (2009) and Vergani et al. (2009). The plan of this paper is the following: in Sec. 2 we describe the spectroscopic and photometric datasets and the derived properties we used to characterise different galaxy populations; in Sec. 3 we derive the GSMFs and in Sec. 4 we analyse the different contribution of galaxy types to the GSMF in different environment,

discussing the implications for the picture of galaxy evolution in Sec. 5.

Throughout the paper we adopted the cosmological parameters $\Omega_m = 0.25$, $\Omega_\Lambda = 0.75$, $H_0 = 70 \text{ km s}^{-1} \text{ Mpc}^{-1}$ and magnitudes are given in the AB system.

2. Data

The zCOSMOS survey (Lilly et al. 2007) is a redshift survey intended to measure the distances of galaxies and AGNs over the COSMOS field (Scoville et al. 2007b). The whole field of about 2 deg^2 has been observed from radio to X-ray wavelengths by parallel projects, involving worldwide teams and observatories. The starting point has been the largest HST survey carried out up to now with ACS. The coexistence of multi-wavelength observation, morphologies, spectroscopic redshifts make COSMOS a unique opportunity to study the evolution of galaxies in their large scale structure context.

2.1. Spectroscopy

The spectroscopic survey zCOSMOS is currently on-going and is subdivided in 2 different parts: the “bright” survey, aiming at observing ~ 20000 galaxies, with a pure flux limited selection corresponding to $15 \leq I_{AB} \leq 22.5$, and the “deep” survey, whose goal is the measure of redshifts in the range $1.4 \leq z \leq 3.0$, within the central 1 deg^2 .

The data used in this paper belong to the so-called 10k sample (Lilly et al. 2009), consisting of the first 10644 observed objects of the “bright” survey, over an area of 1.402 deg^2 with a mean sampling rate of $\sim 33\%$. The final design of the survey aims at reaching a sampling rate of $\sim 60 - 70\%$, achieved by means of an eight-pass strategy. The observations have been carried out with VIMOS@VLT with the red grism at medium resolution $R \sim 600$. The data have been reduced with VIPGI (Scodreggio et al. 2005) and spectroscopic redshifts have been visually determined after a first hint provided by EZ (Garilli 2009)¹. The reliability of the redshift measurements has been represented by means of a flag: a 4 value corresponds to 100% confidence, 3 to $\sim 90\%$, 2 to $\sim 75\%$, 1 to $\sim 50\%$ and 0 to a non measured redshift. All the redshifts have been checked by more than two astronomers. A decimal digit specifies if the redshift is in agreement with photometric redshifts (Feldmann et al. 2006) computed from optical and near infrared (NIR) photometry using the code ZEBRA (Zurich Extragalactic Bayesian Redshift Analyzer, Feldmann et al. 2008). Moreover for some objects the measure resulted to be hampered by technical reasons (for instance the spectrum at the edge of the slit); in those cases a flag -99 has been assigned. Different flags have been assigned to identify broad line AGNs and targets observed by chance in slits.

2.2. Photometry

The photometry used in the following is part of the COSMOS observations and encompasses optical to NIR wavelengths: u^* and K_s from CFHT, B_J , V_J , g^+ , r^+ , i^+ and z^+ from Subaru, and Spitzer IRAC magnitudes at 3.6 , 4.5 , $5.8 \mu\text{m}$. Details on photometric observations and data reduction are given in Capak et al. (2007b); McCracken et al. (2009). The scantiness of standard stars in photometric observations and the uncertainty in the

knowledge of the filter responses result in an uncertain calibration of zero-points. To avoid this inconvenience, we optimized the photometry by applying offsets to the observed magnitudes: we computed such photometric shifts in each band minimizing the differences between observed magnitudes and reference ones computed from a set of Spectral Energy Distributions (hereafter SEDs). We adopted an approach similar to Capak et al. (2007b, see their Table 13), but considering the same set of SEDs we used to compute stellar masses detailed in Sec. 2.3, obtaining in general very similar offsets for all the filters.

2.3. Stellar masses

Stellar masses have been evaluated by means of a SED fitting technique, using the code *Hypermass*, a modified version of the photometric redshift code *Hyperz* (Bolzonella et al. 2000). In a recent paper, Marchesini et al. (2008) analysed the effect of random and systematic uncertainties of the stellar mass estimates on the GSMF, considering the influence of metallicity, extinction law, stellar population synthesis model, and initial mass function. Here we describe the approach and the tests we performed on our data.

We used different libraries of SEDs, derived from different models of stellar population synthesis: 1. the well-known Bruzual & Charlot (2003, hereafter BC03) library, 2. Maraston (2005, hereafter M05) and 3. Charlot & Bruzual (2009, hereafter CB07). The main difference among the three libraries is the treatment of thermally pulsing asymptotic giant branch (TP-AGB) stars. M05 models include the TP-AGB phase, calibrated with local stellar populations. This stellar phase is the dominant source of bolometric and near-IR energy for a simple stellar population in the age range 0.2 to 2 Gyr. Summing up the effects of both overshooting and TP-AGB, the M05 models are brighter and redder than the BC03 models for ages between ~ 0.2 and ~ 2 Gyr (Maraston et al. 2006). The use of the M05 models implies the derivation of lower ages and stellar masses for galaxies in which the TP-AGB stars are significantly contributing to the observed SED (i.e., ages of the order of ~ 1 Gyr). At older ages the M05 models are instead bluer. CB07 is the first release of the new version of the Charlot & Bruzual library, not yet public. CB07 models include the prescription of Marigo & Girardi (2007) for the TP-AGB evolution of low and intermediate-mass stars. Similarly to M05 models, this assumption produces significantly redder near-IR colors, and hence younger ages and lower masses, for young and intermediate-age stellar populations. A brief description of the effect on GSMFs induced by different choices of template SEDs can be found in the companion paper by Pozzetti et al. (2009).

All the considered libraries provide a Simple Stellar Population (SSP) and its evolution in many age steps for a fixed metallicity and a given Initial Mass Function (IMF); it is possible from the SSP models to derive the composite stellar populations that can reproduce the different types of observed galaxies, imposing a star formation history (SFH). We built 10 exponentially declining SFHs with e -folding times ranging from 0.1 to 30 Gyr plus a model with constant star formation. Smooth SFHs are a simplistic representation of the complex SFHs galaxies can have experienced. Nonetheless in Pozzetti et al. (2007) we also computed stellar masses using SEDs with random secondary bursts superimposed to smooth SFHs, finding differences well within the statistical uncertainties for most of the sample. Instead, for a minor subsample of galaxies, stellar masses obtained using models with secondary bursts can become $\sim 40\%$ larger, although the effect on the final GSMF remains negligible.

¹ both VIPGI and EZ are public softwares retrievable from <http://cosmos.iasf-milano.inaf.it/pandora/>

The IMF is another important parameter: differences between stellar mass estimates derived with different underlying IMFs can be statistically recovered. The most used IMFs are the Salpeter (Salpeter 1955), Kroupa (Kroupa 2001), and Chabrier (Chabrier 2003) ones. The statistical differences of stellar masses is $\log M_{\text{Salp}}^* \approx \log M_{\text{Chab}}^* + 0.23$, $\log M_{\text{Chab}}^* \approx \log M_{\text{Krou}}^* - 0.04$. Besides the mass, the best fit SEDs obtained with 2 different IMFs can correspond to significantly different values for other parameters used in the SED fitting process.

In stellar population synthesis models the metallicity can be evolving or fixed. We have verified in simulated catalogues that introducing different values of metallicities does not introduce a substantial improvement of the quality of the best fits, at the cost of the introduction of an additional parameter. Consequently we adopted a fixed solar metallicity, even though this choice may introduce another small uncertainty on the stellar mass estimate.

Dust extinction has been modeled by means of the Calzetti's law (Calzetti et al. 2000), with values ranging from 0 to 3 magnitudes of extinction in V band.

The χ^2 minimization comparing observed and template fluxes at a fixed redshift $z = z_{\text{spec}}$ provides the best fit SED, to which are associated a number of physical parameters, like the age, the reddening, the instantaneous star formation and the stellar mass. Notice that the meaning of stellar mass throughout this paper is not the integral of the star formation, because from that value we have to exclude the return fraction, i.e., the fraction of gas processed by stars and returned to the interstellar medium (ISM) during their evolution.

Tests on simulated catalogues considering the effect on stellar mass estimates of different choices of reddening law, SFHs, metallicities, SED libraries show a typical dispersion of the order of $\sigma_{\log M} \approx 0.20$. Even a simpler technique like the one used by Maier et al. (2009) and derived from Eq. 1 of Lin et al. (2007), produces a scatter not larger than ~ 0.16 dex, although with some small trend as a function of stellar mass and redshift. These tests show that stellar mass is a rather stable parameter in SED fitting when dealing with a set of data spanning a wide wavelength range extended up to NIR.

Since the fluxes provided by the available libraries at IR wavelengths are extrapolated, the choice of filters used in best fitting is reduced to $2.5 \mu\text{m}$ rest-frame for M05 models (at longer wavelengths these models are using the Rayleigh-Jeans tail extrapolation) and to $5 \mu\text{m}$ rest-frame for BC03 and CB07 models, since at longer wavelengths also the dust re-emission can contribute to the flux budget.

A problem arising when dealing with a very large number of template SEDs is to avoid non-physical best fits. We applied 2 priors (the same used in Pozzetti et al. 2007, and proposed by Fontana et al. 2004 and Kauffmann et al. 2003) to avoid such a problem. In particular, we excluded best fit SEDs not fulfilling the following requirements: 1. $A_V \leq 0.6$ if $\text{age}/\tau \geq 4$ (i.e., old galaxies must have a moderate dust extinction); 2. star formation must start at $z > 1$ if $\tau < 0.6$ Gyr. Moreover, we tested through simulations that imposing a minimum best fit age of 0.09 Gyr reduces potential degeneracies and improves the reliability of the stellar mass estimate. The maximum allowed age is the age of the Universe at z_{spec} .

As mentioned in Sec. 2.2, the first SED fitting run over the brightest galaxies and most secure galaxy redshifts has been performed to compute the photometric offsets. We checked that further iterations of the SED fitting and offset estimation do not improve significantly the χ^2 statistics.

To ease the comparison with literature results, in the following we present GSMFs obtained adopting the BC03 stellar

masses. However the qualitative trends are the same for any choice of the stellar population synthesis models.

2.4. Environment

The density field has been derived for the 10k spectroscopic sample using different estimators combined with the ZADE (Zurich Adaptive Density Estimator, Kovač et al. 2009) algorithm. Most of the existing studies rely on photometric redshifts and projected densities computed in wide redshift slices, possibly diluting the signal from overdense regions. An important added value of COSMOS is the availability of spectroscopic redshifts obtained with a good sampling rate, making feasible an accurate estimate of the environment, with high resolution also on the radial direction.

To this aim, spectroscopic redshifts have been used as a skeleton of galaxy structures, with the incorporation of a statistical treatment of the likelihood function of photometric redshifts computed with ZEBRA. This approach allows to probe a wide range of environments and to reduce the Poisson noise. Results have been extensively and carefully tested on mock catalogues from the Millennium simulation (Kitzbichler & White 2007). The reconstruction of overdensities $1 + \delta$ has been explored using different tracer galaxies, different spatial filters and different weights (e.g., luminosity or stellar mass) assigned to each galaxy. The density contrast δ is defined as $(\rho - \bar{\rho})/\bar{\rho}$, where ρ is the density as a function of RA, DEC and z and $\bar{\rho}$ is the mean density measured at the same redshift. In principle, the fully realistic physical representation of the environment should involve the mass of the dark matter haloes in which the galaxies are embedded. This mass is clearly not directly accessible to observations, hence an affordable surrogate to weight the number density field is given by the stellar masses of the surrounding galaxies. This is a proxy of the overall density field, since galaxies are biased tracers of the underlying matter distribution, and stellar mass lacks the gas component that differentiates red and blue galaxies. Since the choice of a fixed selection band results in different populations preferentially sampled at different redshifts, weighting with stellar mass should also mitigate this issue. As expected, mass weighted overdensities have an increased dynamical range, in particular at the highest densities. As we will see in Sec. 3.5, this procedure, although physically motivated, can introduce some spurious signal, mainly induced by the mass of the galaxy around which the overdensity is computed.

Another estimate of the high density environments in which galaxies reside can be obtained by selecting optical groups, as described in Knobel et al. (2009), or X-ray ones (Finoguenov et al. 2007; Finoguenov et al. 2009); low density environments can be tracked by isolated galaxies defined using their Voronoi volumes, as in Iovino et al. (2009). The two determinations of the environment are in a fairly good agreement, considering the differences of the involved scales (Kovač et al. 2009).

In the following we use as reference the 5th nearest neighbour estimator (hereafter 5NN) of the density field, which represents a good compromise between the smallest accessible scales and the reliability of the overdensity values. In this approach, tracer galaxies are considered within $\pm 1000 \text{ km s}^{-1}$ from the central galaxy and counted, after distance sorting, until their number becomes larger than 5, considering also the fractional contribution from objects with photometric redshifts, derived from their likelihood function. Overdensities are then computed at the position of each galaxy in the spectroscopic sample, considering also the contribution to the number or mass density of the

galaxy itself. We checked that the same qualitative trends of the GSMFs analysed in the following are present also when considering other estimators.

2.5. Galaxy type classification

Galaxy types can be classified in a multitude of ways, using their rest-frame colours, their SEDs, their spectroscopic features, their structural parameters and their morphologies, all of them derivable with different methods. Different classifications map different physical properties. For instance, the rest-frame colour $U - B$ and the galaxy SED are used as a proxy of the star formation activity and history, the morphology is an indicator of the dynamical state, and the two are not completely overlapping (Mignoli et al. 2009).

Even if COSMOS offers a profusion of methods to group galaxies, we have chosen to use only two types of classification: photometric and morphological.

The photometric type is defined by SED fitting over the optical magnitudes, assuming as reference the same templates used by Ilbert et al. (2006): the 4 locally observed CWW (Coleman et al. 1980) and two starburst SEDs from Kinney et al. (1996), extrapolated at UV and mid-IR wavelengths. These six templates are then interpolated to obtain 62 SEDs and optimized with VVDS spectroscopic data. The SED fitting, a χ^2 minimization performed with the code ALF (Ilbert et al. 2005; Zucca et al. 2006, 2009), gives in output the best fit. Galaxies are then classified in 4 types, closely corresponding to colours of ellipticals (type 1), early spirals (type 2), late spirals (type 3) and irregular and starburst galaxies (type 4). We group photometric types 2, 3 and 4 in a single class, to explore in a simple way the evolution of the early and late-type bimodality.

As morphological classification we adopted the one presented in Scarlata et al. (2007): the availability of deep F814-band ACS@HST images over the whole COSMOS field (Koekemoer et al. 2007) allows a good determination of the structural parameters on which the morphology derived with the software ZEST (Zurich Estimator of Structural Types, Scarlata et al. 2007) is based. The method is a PCA analysis using estimates of asymmetry, concentration, Gini coefficient, M_{20} (the second order moment of the 20% brightest pixels) and ellipticity. The morphological classes are the following: early type (type 1), disk (type 2, with an associated sub-classification ranging from 0 to 3 representing the “bulgeness”, derived from the n Sérsic indices, Sargent et al. 2007) and irregular galaxies (type 3). Adopting the same line of reasoning used for the photometric types, we grouped morphologically classified galaxies in two broad classes, with early type including classes 1 and 2.0, i.e., ellipticals and bulge dominated galaxies.

3. Mass Functions

3.1. The sample

Not all the spectroscopic redshifts have the same level of reliability, as explained in Sec. 2.1. The sample we used includes only the galaxies with flags corresponding to most secure redshifts, i.e., starting from flag = 1 in case of agreement with photometric redshifts. In detail, we excluded from our sample broad line AGNs ($\sim 1.8\%$ of the statistical sample), stars ($\sim 5.9\%$), objects with less than 5 detected magnitudes available to compute the SED fitting ($\sim 1.7\%$) and objects for which the ground photometry can be affected by blending of more sources, as derived from the number of ACS sources brighter than $I = 22.5$

within $0.6''$ ($\sim 0.5\%$). The final sample contains 8450 galaxies with redshifts between 0.01 and 2 and 7936 in the redshift range where the following analysis is carried out, $z = 0.1 - 1$.

3.2. Statistical weights

To take into account that the observed galaxies are only a fraction of the total number of possible available targets with the same properties we need to apply statistical weights to each observed object (Zucca et al. 1994; Ilbert et al. 2005). To this aim we computed the weight w_i for each galaxy in our sample as the product of two factors connected to the Target Sampling Rate (TSR) and to the Spectroscopic Success Rate (SSR). Here we outline the basic principles on which the computation is based, referring the reader to Zucca et al. (2009) for further details.

The TSR is the fraction of sources observed in the spectroscopic survey compared to the total number of objects in the parent photometric catalogue from which they are randomly extracted. In the case of zCOSMOS the VMPS tool for mask preparation (Bottini et al. 2005) has been set in such a way that the objects have been randomly selected without any bias. A different treatment has been granted to compulsory targets, i.e., objects with forced slit positioning: they have a much higher TSR ($\sim 87\%$) compared with the “random” sample ($\sim 36\%$). The associated weight is $w_i^{\text{TSR}} = 1/\text{TSR}$.

The SSR represents the fraction of observed sources with a successfully measured redshift: it is comprehensibly a function of apparent magnitude, being linked to the signal-to-noise ratio of the spectrum, and it ranges from 97.5% to 82% considering the brightest and faintest galaxies, respectively. The weight deriving from the SSR is $w_i^{\text{SSR}} = 1/\text{SSR}$.

The SSR is not only a function of magnitude, but also of redshift, since the spectral features on which the redshift measure relies can enter or go out the observed wavelength window (Lilly et al. 2007). Therefore, the redshift distribution of the measured redshifts can be different from the real one; it is possible to take into account of our lack of knowledge on the failed measures by using photometric redshifts. Hence we used the Ilbert et al. (2009a) release of z_{phot} and computed the SSR in $\Delta z = 0.2$ redshift bins. Moreover, the characteristic emission or absorption lines are different for different galaxy types, as shown in Lilly et al. (2009). We further split the computation of SSR in each redshift bin separating red and blue galaxies, selected on the basis of their rest-frame $U - V$ colour. The so-called secondary targets, i.e., objects in the parent catalogue, but fallen in the slit by chance, have been considered separately: they are characterised by a lower SSR because they are often located at the spectrum edge or observed only at their outskirts. We computed and assigned the final weights $w_i = w_i^{\text{TSR}} \times w_i^{\text{SSR}}$ considering all the described dependencies.

3.3. Mass Function methods

To compute the GSMFs we adopt the usual non-parametric method $1/V_{\text{max}}$ (Avni & Bahcall 1980), from which we derive the best fit Schechter function (Schechter 1976). The observability limits inside each redshift bin, z_{min} and z_{max} , have been computed for each galaxy from its best fit SED.

As in Pozzetti et al. (2009), we estimated the parametric fit of the GSMFs with both a single Schechter function, like in most published results, and with the sum of 2 Schechter functions, that seems to be statistically required by the data at least in the lowest redshift bins. We adopted the formalism introduced by

Baldry et al. (2004, 2006) using a single M^* to limit the number of free parameters:

$$\phi(M)dM = \phi_1^* \left(\frac{M}{M^*} \right)^{\alpha_1} \exp \left(-\frac{M}{M^*} \right) d\frac{M}{M^*} + \phi_2^* \left(\frac{M}{M^*} \right)^{\alpha_2} \exp \left(-\frac{M}{M^*} \right) d\frac{M}{M^*}. \quad (1)$$

Up to now the need of modeling a faint-end upturn has been mainly pointed out in LF studies, both in field (Zucca et al. 1997) and in rich clusters (Popesso et al. 2007; Jenkins et al. 2007). The departure of the GSMF from a single Schechter function at small stellar masses has been noticed by Baldry et al. (2006, 2008) and Panter et al. (2004) on SDSS. At higher redshifts an *a posteriori* look at the published GSMFs often reveals such an upturn.

We called M_{\min} the lowest mass at which the GSMF can be considered reliable and not affected by incompleteness on M/L (see Ilbert et al. 2004; Pozzetti et al. 2007). A complete description of the procedure can be found in Pozzetti et al. (2009). Basically, the aim is to recover the stellar mass up to which all the galaxy types significantly contributing to the GSMF can be observed. We derived such a value in small redshift slices considering the 20% faintest galaxies, i.e., the ones contributing to the low-mass end of the GSMF. For each galaxy of this subsample we computed the “limiting mass”, that is the stellar mass that the object would have had at the limiting magnitude of the survey, $\log M_{\lim} = \log M + 0.4(I - 22.5)$. For each redshift bin we define as minimum mass the value corresponding to 95% of the distribution of limiting masses and we smooth the M_{\min} vs z relation by means of an interpolation with a parabolic curve. We adopt as minimum stellar mass up to which we can reliably compute the GSMF in each considered redshift bin the M_{\min} at the lowest extreme of the interval, since the $1/V_{\max}$ method corrects the residual volume incompleteness. When dealing with GSMFs divided per galaxy types, the minimum masses are obtained using the considered subsample.

It should be noticed that this limit substantially decreases the number of objects considered in each redshift bin to derive the GSMF. The redshift intervals [0.10, 0.35], [0.35, 0.50], [0.50, 0.70] and [0.70, 1.00] were chosen to contain a similar number of galaxies.

3.4. The choice of the environment definition

As mentioned in Sec. 2.4, the density field of the COSMOS field (see Kovač et al. 2009) has been reconstructed for different choices of filters (fixed comoving aperture or adaptive with a fixed number of neighbours), tracers (flux limited or volume limited subsamples) and weights (stellar mass, luminosity or no weight, i.e., considering only the number of galaxies).

We tested the options that allow an unbiased comparison over the whole redshift range, from $z = 0.1$ to 1.0. In particular, we explored the 5NN estimator and the 5NN mass weighted one (hereafter 5NNM), both of them computed using volume limited tracers, with two choices of luminosity limits: $M_B \leq -20.5 - z$ (bright tracers) and $M_B \leq -19.3 - z$ (faint tracers), where M_B is the absolute magnitude in the B band computed with ZEBRA. The absolute magnitude cut has been derived considering the distribution of absolute magnitudes vs redshift, the so-called Spaenhauer diagram (Spaenhauer 1978), and the evolution of the parameter M_B^* of the LFs (Zucca et al. 2009). The requirement of two different limits arises from the rareness of bright tracers at low redshift and the incompleteness of faint tracers at high

redshift; for this reason the two overdensity estimates cannot be computed over the whole redshift range, but only at [0.1, 0.7] and $z = [0.4, 1.0]$ for faint and bright tracers respectively.

3.4.1. The effect of environment tracers on GSMF

Two issues are troubling the study on the evolution of GSMFs as a function of environment and must be solved: 1. we have to understand if the 5NNM estimator is a better tracer of the environment, as presumed from the theoretical point of view; 2. we have to be sure that the use of two different tracers, e.g., with a change at $z = 0.7$, does not introduce a spurious signal that can be misinterpreted as an evolutionary trend.

To answer both questions we used as test case the redshift interval [0.4, 0.7], where all the estimates are available, and we computed the quartiles of the $1 + \delta$ distribution in this redshift bin considering only the objects with masses larger than the minimum mass. Henceforth, we will refer to the lowest and highest quartiles of $1 + \delta$ as D1 and D4 respectively. In the rest of the paper we will focus our study on these two extremes.

In Fig. 1, panel (a), we show the comparison of the GSMFs, using a single Schechter function fit, for 5NN and 5NNM overdensity estimators, both using the faint volume limited tracers. The separation of GSMFs between D1 and D4 environments is more prominent when considering the mass weighted estimator, because of the larger dynamical range of probed $1 + \delta$ values. In particular, the main difference is in the massive part of D1 GSMF: massive galaxies in low density environments using 5NN are moved to intermediate densities for 5NNM estimator because of their large stellar masses. This decreases the number (and therefore the normalisation of the GSMF) of massive galaxies in low density environment when the 5NNM estimator is adopted. To test if this enhancement of the difference between the D1 and D4 GSMFs is a reliable effect, we performed the following test: we removed the mass-density relation by shuffling the original catalogue and computing overdensities considering objects with their original coordinates, but assigning to each one the observed properties (magnitudes, stellar mass, weight) of the 25th following object after redshift sorting. Both 5NN and 5NNM overdensities and their quartiles have been recomputed, since the shuffling implies also a change of tracers. The choice of the 25 object jump is a compromise between the requirements of preserving a similar probability to be observed at the chosen redshift (i.e., avoiding unphysical galaxy properties if a big jump in redshift is allowed) and selecting objects possibly not in the same structure, where we know galaxies share similar properties. We expected that, randomizing the contribution of stellar mass, the 5NN and 5NNM GSMFs would become consistent with each other. The comparison between GSMFs with 5NN and 5NNM “shuffled” overdensities is shown in Fig. 1, panel (b): a difference between GSMFs in different environments is still present at high masses, now more evident in the high density environment.

The last test we carried out to understand this residual signal was the removal of the central galaxy when computing $1 + \delta$ from the original catalogue: the comparison of the resulting GSMFs is in Fig. 1 panel (c), showing now fully consistent GSMFs at high and low densities as defined from 5NN and 5NNM estimators.

These tests seem to indicate that the mass weighting scheme assigns too much importance to the stellar mass at scales of the order of the galaxy itself. Then, to avoid any possible bias due to stellar mass over-weighting, despite its physically motivated link with the halo mass, we discarded the 5NNM estimator and performed our analysis using number weighted overdensities.

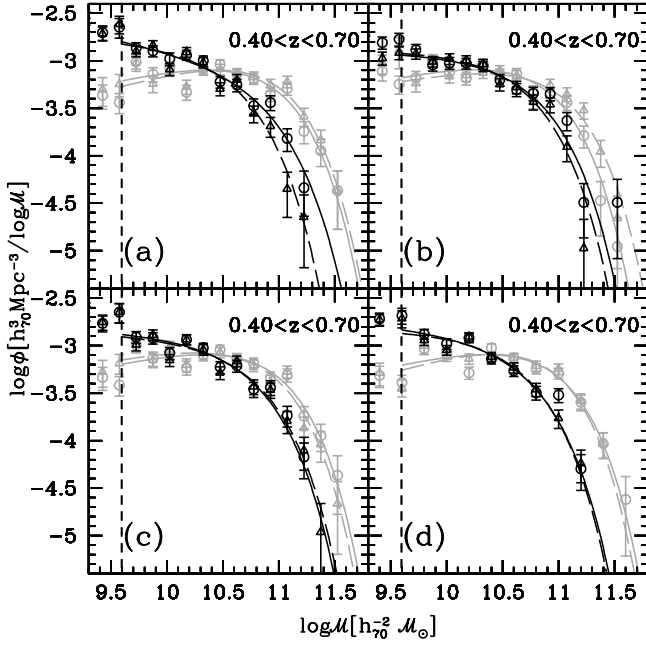


Fig. 1. (a) Comparison of GSMFs for environment estimates from 5NN and 5NNM volume limited with faint tracers: Black: D1 (underdense); Gray: D4 (overdense). Solid line and empty dots: 5NN. Dashed line and empty triangles: 5NNM. The vertical dashed line represent the value of M_{\min} at $z = 0.4$. (b) Like panel (a), but 5NN and 5NNM overdensities have been estimated after a random shuffling of galaxy properties to remove the mass-density relation. (c) Like panel (a), but 5NN and 5NNM overdensities have been estimated without considering the properties of the central galaxy. (d) GSMFs for bright ($M_B \leq -20.5 - z$, dashed lines and empty triangles) and faint ($M_B \leq -19.3 - z$, solid lines and empty dots) tracers using 5NN overdensities in the D1 (black) and D4 (gray) environments.

Approaching the second problem, we would like to test if the change of the tracers at $z = 0.7$ may introduce some change in the GSMF, at risk of possible confusion with the evolution. We already know that the scales probed at the same $1 + \delta$ are more or less twice as large for bright compared to faint tracers (Kovač et al. 2009), therefore it is not possible to use the same $1 + \delta$ threshold using faint and bright tracers. To overcome this problem we determined the quartiles of $1 + \delta$ separately for each redshift bin. The result of this test is shown in panel (d) of Fig. 1. In the $z = 0.4 - 0.7$ bin, where both the tracers are available, the GSMFs obtained with the two tracers, with independently computed quartiles, are completely consistent with each other in under and overdense environments D1 and D4, and therefore we assume we can safely compare the results at redshifts $z < 0.7$ computed with faint tracers to those computed at $z \geq 0.7$ with the bright ones.

3.4.2. Definition of overdensity quartiles

As already mentioned, to trace the effect of extreme environments on the evolution of galaxies we considered the quartiles D1 and D4 of the $1 + \delta$ distribution, using 5NN volume limited overdensities. The quartiles have been computed at each redshift bin considering only the population of galaxies more massive than M_{\min} of the highest redshift bin, to ensure that such

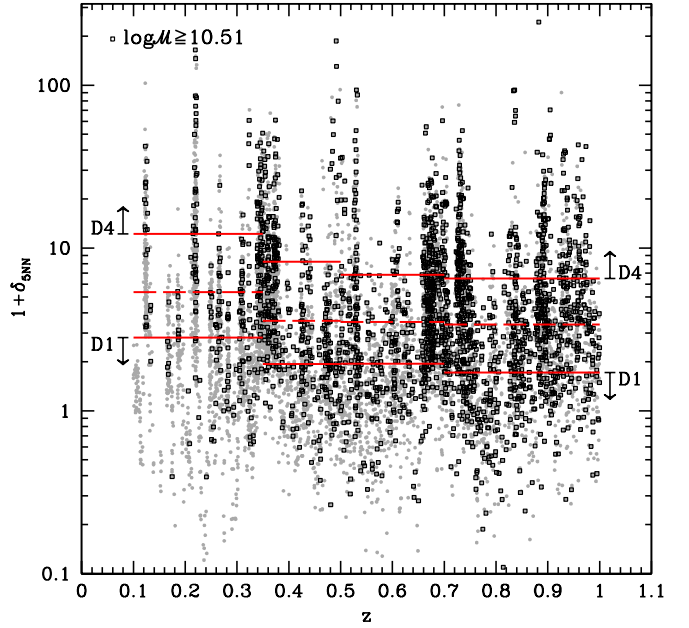


Fig. 2. Definition of quartiles for the 5NN estimator using volume limited tracers: gray points represent the full sample, black squares the galaxies with masses above the M_{\min} computed in the last redshift bin, horizontal segments show the values of the quartiles of $1 + \delta$ computed from the distribution of these massive galaxies, the dashed ones indicate the median.

a definition is not affected by the variation as a function of redshift of the observable mass range, populated by different mix of galaxy types. The quartiles definition used throughout this paper is shown in Fig. 2. The median scales probed by the 5th nearest neighbour range from $0.87 \text{ Mpc } h_{70}^{-1}$ in the D4 environment at low redshift to $7.57 \text{ Mpc } h_{70}^{-1}$ in the D1 quartile at the highest redshift bin, where we are forced to use bright tracers.

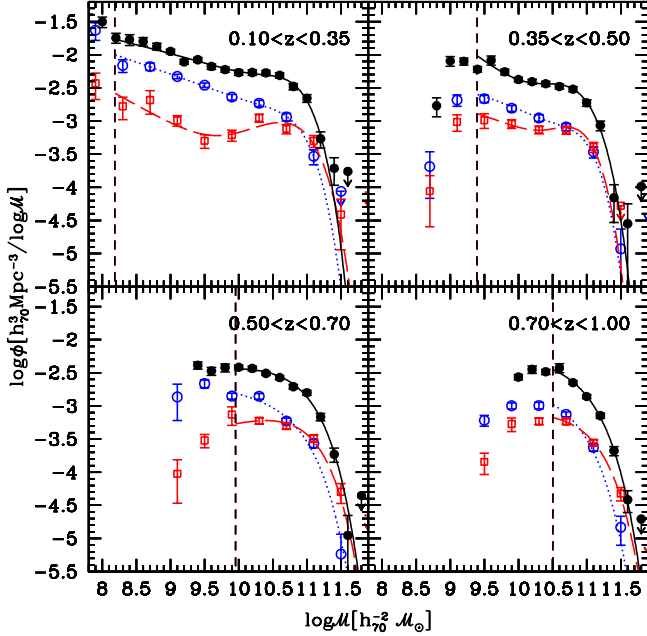
The trend toward higher values of overdensity at lower redshifts is in some measure expected from the growth of structures, which is amplifying the dynamic range of overdensities, but this increase cannot be quantified through the linear approximation, not valid on the scales probed by our density estimates. The different values of the $1 + \delta$ quartiles in the different redshift bins correspond to very similar scales when the same tracers are used.

3.5. Mass Functions in different environments

The GSMFs in the two extreme environments are shown in Fig. 3: the bimodality already visible in the global GSMFs (Pozzetti et al. 2009, see also the points and lines in Fig. 3), with an upturn of the low-mass end around $M \sim 10^{9.5} M_{\odot}$, is much exacerbated in the high density regions, at least in the two lowest redshift bins. We used the double Schechter function fit only up to $z \sim 0.5$, where the dip of the GSMFs falls at stellar masses larger than M_{\min} . Because of the choice of the environment definition, the normalisation of D1 and D4 GSMFs does not have a clear physical meaning, since the volumes occupied by each galaxy are referred to the total volume of the survey and the number of galaxies in each environment is not $1/4$ of the total sample. To have a more meaningful definition of the normalisation we should compute the volume occupied by the structures having the considered ranges in $1 + \delta$; here

Table 1. Parameters of the GSMF in the low and high-density environments.

	z	α_1	α_2	$\log \mathcal{M}^*/M_\odot$	ϕ_1^*/ϕ_2^*
D1	0.10 – 0.35	-1.35	+0.14	10.53	1.61
	0.35 – 0.50	-1.25	+0.82	10.52	0.79
	0.50 – 0.70	-1.13	...	10.82	...
	0.70 – 1.00	-1.12	...	10.80	...
D4	0.10 – 0.35	-1.80	-0.33	10.76	0.01
	0.35 – 0.50	-1.28	+0.95	10.52	0.50
	0.50 – 0.70	-0.70	...	10.92	...
	0.70 – 1.00	-0.90	...	10.98	...

**Fig. 3.** The MFs in the extreme quartiles D1 and D4 of the 5NN volume limited overdensities. Black: total GSMF, with $1/V_{\max}$ dots and their Poissonian error bars and Schechter function fit (double Schechter function in the first two redshift ranges and a single one at higher redshifts). Blue: lowest $1 + \delta$ quartile. Red: highest density quartile.

we are interested in the comparison of the GSMF shapes and hence we defer a more in-depth study of the normalisation to a future analysis. A striking difference in GSMFs shapes is evident, with massive galaxies preferentially residing in high density environments, characterised on average by a larger \mathcal{M}^* , and with a steeper slope than D1 GSMFs at $z \geq 0.35$. The different shapes and the strong bimodality in the D4 GSMF can be explained like the global one (Pozzetti et al. 2009) by the different contribution of different galaxy types, as we will see in the next Section. The parameters of the Schechter fits to the GSMFs are listed in Table 1.

4. Evolution of galaxy types in different environments

The need of a double Schechter function to fit the global and environment-selected GSMFs at least up to $z \sim 0.5$ can be linked to the contribution of different galaxy populations. Galaxies with the same luminosity can be characterised by very different \mathcal{M}/L ,

Table 2. Parameters of the GSMF for the two photometric types in the low and high-density environments. The ratio (column still to be filled) is computed assuming a single Schechter function also for the GSMF not splitted in different classes.

	z	α_1	$\log \mathcal{M}^*/M_\odot$
D1T1	0.10 – 0.35	-0.33	10.60
	0.35 – 0.50	-0.17	10.72
	0.50 – 0.70	-0.90	10.93
	0.70 – 1.00	-0.70	10.65
D1T2	0.10 – 0.35	-1.41	10.71
	0.35 – 0.50	-1.51	10.81
	0.50 – 0.70	-1.45	10.70
	0.70 – 1.00	-0.84	10.45
D4T1	0.10 – 0.35	-0.03	10.68
	0.35 – 0.50	-0.23	10.82
	0.50 – 0.70	-0.28	10.87
	0.70 – 1.00	-0.15	10.94
D4T2	0.10 – 0.35	-1.39	10.92
	0.35 – 0.50	-1.43	11.02
	0.50 – 0.70	-1.30	10.74
	0.70 – 1.00	-0.03	10.30

and this is why it is harder to see such a bimodal shape in LFs, despite this effect has been first detected in LFs, because of the longer history of this kind of statistical description of galaxy samples.

To study the contribution of galaxies with different photometric types and morphologies in the extreme environments, we computed the GSMFs in D1 and D4, defined as in Sec. 3.5, splitting each sub-sample in galaxy classes. The values of \mathcal{M}_{\min} have been computed separately for early/ellipticals/bulge dominated and late/spirals/disc dominated galaxies. These values are significantly different, especially at low redshift, confirming the very different distributions of \mathcal{M}/L .

The results for the contribution of different photometric types to D1 and D4 GSMFs are presented in Fig. 4, with the best fit parameters of single Schechter function fits in Table 2. Dividing the sample in the two broad morphological classes results in qualitatively similar GSMFs.

Looking at the plots in Fig. 4, it is now manifest that the stronger bimodality in the first two redshift bins in the D4 GSMF is primarily due to the larger contribution of early type galaxies. Just like the global GSMF, in both the considered environments early type galaxies are dominant at high masses ($\log \mathcal{M}/M_\odot \gtrsim 10.7$), while their contribution rapidly decreases at intermediate masses. On the other hand, late type galaxies, being described by much steeper GSMFs, start to dominate at intermediate and low masses ($\log \mathcal{M}/M_\odot \sim 10$).

In addition to the relative contribution of different galaxy types is different in D1 and D4, it is sensible asking the question if the shape of the GSMFs of galaxies of the same type is the same in different environments, i.e., if there exists a “universal” mass function of early/late type galaxies. In Fig. 5 we show the comparison of early type and late type GSMFs in the two environments, in each redshift bin renormalised with the number density computed for masses $\geq \mathcal{M}_{\min}$. Some small difference on the shape of the GSMFs is present, with a trend toward a slightly higher density of massive galaxies in overdense regions, but the similarity of the GSMFs in all the redshift bins and of both the photometric types is remarkable and somewhat unexpected. From the plots in Fig. 5 we may argue that a quasi-universal GSMF characterise the different galaxy types, disregarding their environment.

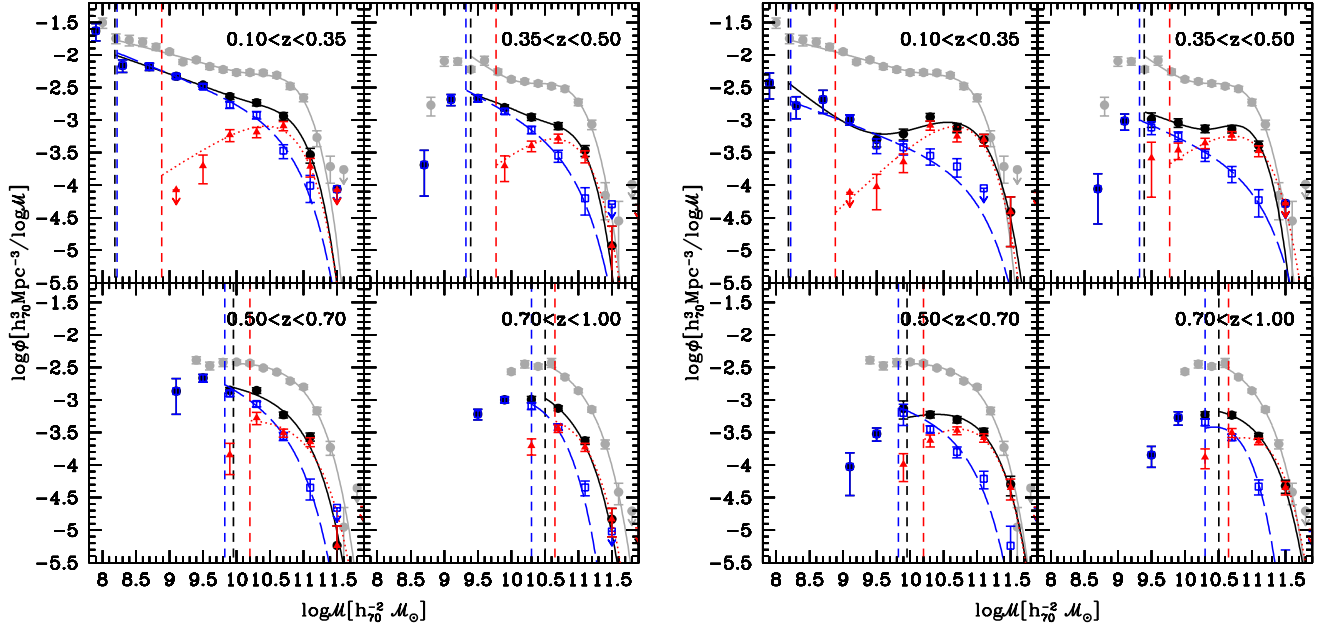


Fig. 4. Left: quartile D1 (low density environment). Right: quartile D4 (high density). Gray: total GSMF. Black: MF relative to the considered quartile. Red triangles and dotted lines: early photometric type galaxies. Blue squares and dashed lines: late photometric type galaxies. At high masses the upper limit points show the 2σ confidence limits for 0 detections following Gehrels (1986).

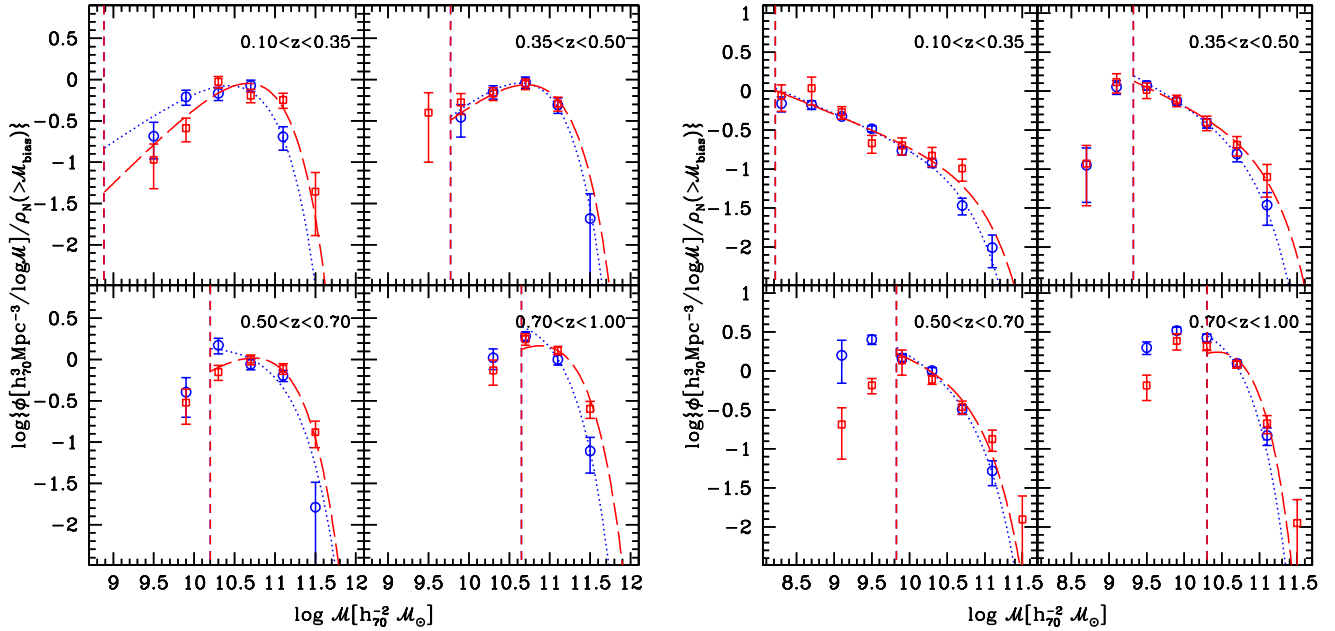


Fig. 5. Left: GSMFs of photometrically early type in D1 and D4 environments, renormalised to number density = 1 for stellar masses $> M_{\min}$. Right: the same for photometrically late type galaxies. Blue dotted lines and circles represent the GSMFs in underdense regions, D1. Red dashed lines and squares illustrate D4 GSMFs.

To examine the differential contribution of various galaxy types in different environments we can compute the evolution of the ratio between the GSMF of a given galaxy class and the global GSMFs in each environment. In Fig. 6 we show the ratio of $1/V_{\max}$ estimates of early type GSMF in over and underdense regions for the two extreme redshift bins. The trend for late type galaxies is reversed with respect to the one shown in the figure. The error bars have been computed with a Montecarlo simula-

tion considering Gaussian distribution of errors with rms from Poissonian error bars from $1/V_{\max}$ method. The 16 and 84% of the 100,000 iterations of ratio distribution are reported in the plot as error bars. The vertical dashed line shows the value of M_{\min} for early type galaxies in the redshift bin $z = 0.7 - 1.0$. Despite the large error bars, Fig. 6 illustrates that at the largest redshifts we can probe the fractional contributions of early photometric types to the GSMF in different environments are more

or less the same for D1 and D4 at all the masses we can safely study. On the other hand, the fractional contribution is significantly different at low redshift, mainly at intermediate stellar masses ($\log M/M_\odot \lesssim 10.5$). This trend seems to testify a faster growth in high density environments of the fractional contribution of early type galaxies. At intermediate masses the differences between the two extreme environments are larger: high stellar masses ($\log M/M_\odot \gtrsim 10.7$) are populated only by passive red galaxies in both environments, at lower masses ($\log M/M_\odot \lesssim 10$, where it is possible to probe them) the population of late type/star forming galaxies dominates in all the environments.

In a scenario consistent with these data, showing an increase of early type galaxies with cosmic time, intermediate mass blue galaxies are being transformed in more massive red galaxies, after quenching their star formation in a more efficient way in overdense regions. A possible way to quantify this different evolutionary speed is through the analysis of the evolution with redshift of M_{cross} , representing the mass above which the GSMF is dominated by early-type galaxies. We show such a quantity computed from $1/V_{\text{max}}$ points in Fig. 7 for different photometric types. We can see that since $z \sim 1$, at which the M_{cross} values in low and high density environments were similar, the subsequent evolution produces a significant difference between the two M_{cross} values. The ratio of M_{cross} in the highest and lowest redshift bins implies an evolution of a factor ~ 2 in low density and ~ 4.5 in high density regions. If we consider M_{cross} being the same in the highest redshift bin, the difference in evolution due to the influence of environment, computed as the ratio of the values M_{cross} in the lowest redshift bin, is a factor ~ 3 . From a different point of view, the plot in Fig. 7 is showing that the environment starts to act on the evolution of galaxies at $z \sim 1$, producing in the lowest redshift bin a delay of ~ 2 Gyr in underdense regions to attain the same mix of galaxy types observed in high density regions.

5. Discussion

5.1. The mechanism and timescale of galaxy transformation

Figures 6 and 7 suggest some clues on the timescale and mechanism responsible of galaxy quenching in different environments. We found that the evolution in the high density regions is faster than in low density ones, i.e., the rate of transformation in early photometric types is accelerated from $z = 1$ to low redshifts in overdense regions. The mechanism responsible for quenching the star formation, and then for the transformation of blue galaxies into passive ones, must be environment dependent. The physical processes operating on galaxies and transforming their colours and/or morphologies are manifold and can be internally or externally driven and gravitationally or hydrodynamically induced (see for reviews Boselli & Gavazzi 2006; Treu et al. 2003). The choice of possible mechanisms should exclude the ones acting mainly on galaxy clusters, since only a small fraction of our galaxies are probably located in rich clusters. We can exclude processes like ram-pressure, consisting in the gas stripping of a galaxy moving through a dense inter-galactic medium, with the effect of truncating the star formation, and harassment, i.e. a gravitational interaction in high velocity encounters of galaxies, causing morphological transformation and bursts of star formation. Given the requirements on galaxy velocities and inter-galactic medium density, these processes cannot have a significant impact on the present study.

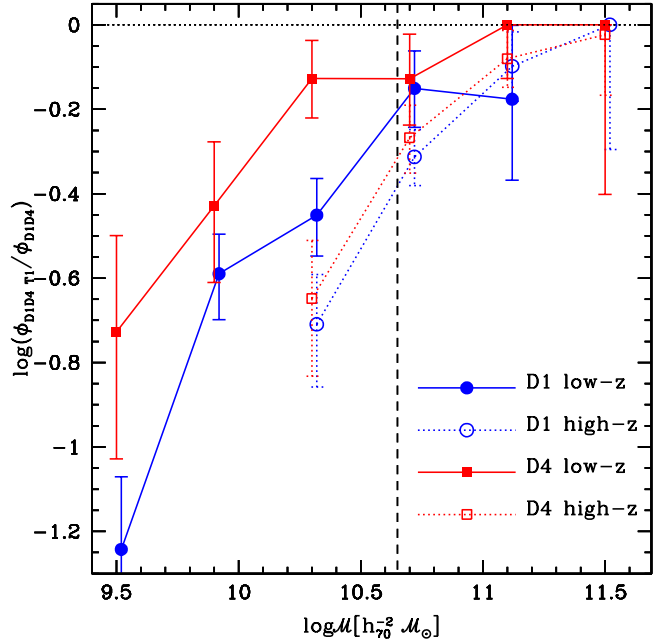


Fig. 6. Evolution of the fractional contribution of the early photometric type to the global MFs (the late type fractional contribution is complementary to the one shown in this plot) in the two extreme environments. Blue lines and circles refer to low density environment D1 (displaced by 0.02 in the abscissa to avoid overlapping), red lines and squares to the high density sample D4. Dotted lines and empty symbols represent the highest redshift bin $z = [0.7, 1.0]$, solid lines and filled points the lowest one, $z = [0.1, 0.35]$. The vertical dashed line marks M_{min} in the high redshift bin (the value at low redshift is outside the plot). Error bars have been computed as 16 – 84% of the distribution of Montecarlo simulations.

Viable mechanisms in the field are instead merging and starvation. Major merging processes can trigger AGN and quench the star formation: the fraction of pairs, related to the rate of merging, can be dependent on environment. The effect of merging is to deplete the low mass end and populate the high mass one with elliptical morphologies. To explain the evolution of the density of massive elliptical galaxies, Ilbert et al. (2009b) found that the rate of wet mergers should steeply decline at $z < 1$. Limits on the contribution of major merging as primary mechanism can be drawn from the evolution of pair fraction (de Ravel et al. 2009b, who found that 20% of the stellar mass in present day galaxies with $\log M/M_\odot > 9.5$ has been accreted by major merging events since $z \sim 1$) and from the GSMF (Pozzetti et al. 2009, who derived an upper limit to the fraction of major merging per Gyr of the order of 20 – 40% for the global population, derived from the GSMF evolved according to the mass growth due to star formation).

Also strangulation (called as well starvation or suffocation), consisting of halo-gas stripping, can play a role: when the diffuse warm and hot gas reservoir in the galaxy corona is stripped because of gravitational interaction with low-mass group-size haloes or with cluster haloes at large distances from the core, the gas cannot be accreted anymore and the galaxy will exhaust the remaining cold gas through the star formation, in a timescale which can be instantaneous or slow, i.e., in few Gyr, depending also on the mass of the galaxy (Wolf et al. 2009). The result is

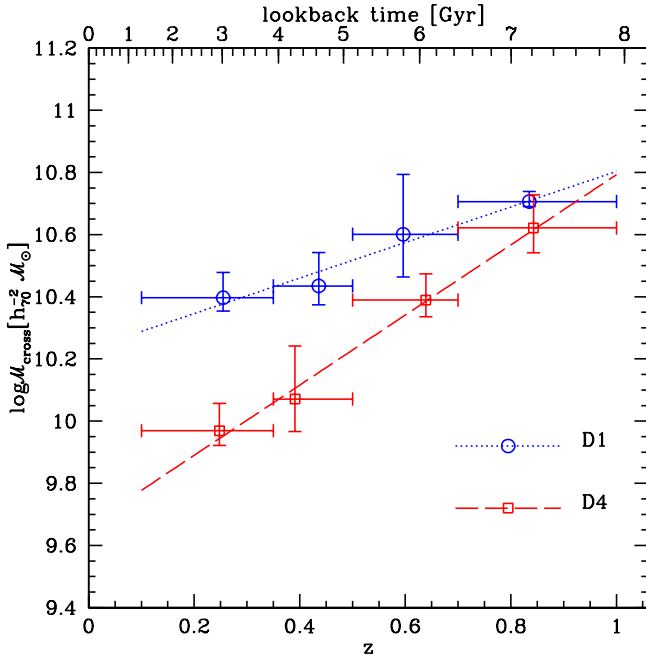


Fig. 7. M_{cross} of photometric types in the extreme quartiles D1 and D4. Blue: low-density environments. Red: high-density. The points are located at the median redshift of the early plus late samples and error bars represent the width of the redshift bin and the error on the GSMF ratio from $1/V_{\text{max}}$ method. A linear fit to the points is also shown.

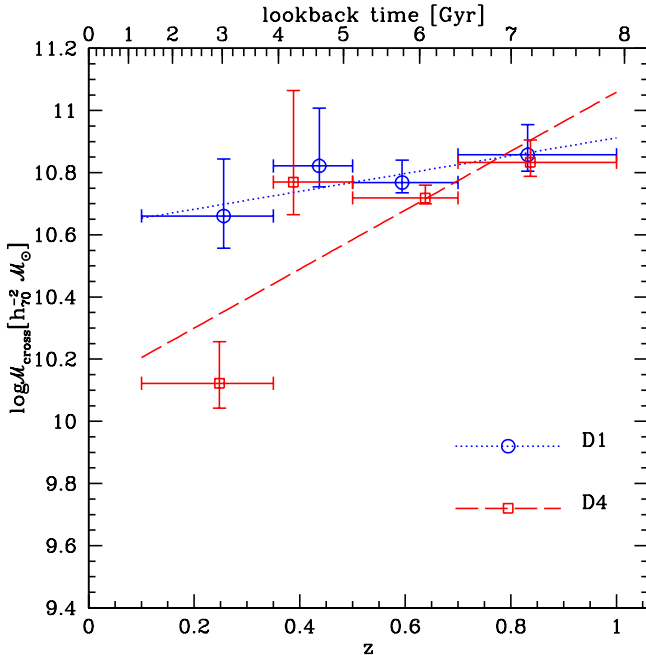


Fig. 8. Like Fig. 7, with M_{cross} computed for morphological types.

the suppression of the star formation, not followed by a morphological transformation, explaining the possible presence of red spirals, even if the fading of the disc can lead to an earlier-type morphological classification.

To further constrain the quest for possible transformation mechanisms, we computed GSMFs also dividing the sample following the morphological classification by Scarlata et al. (2007), as defined in Sec. 2.5. In Fig. 8 we show the values of M_{cross} in the 4 considered redshift bins. This plot appears different from the analogous plot obtained dividing galaxies in photometric types: the values of M_{cross} are higher and their evolution seems insensitive to the environment up to $z \sim 0.4$. The larger values of M_{cross} for morphological classification suggest that the dynamical transformation into elliptical galaxies follows the quenching of the star formation. It is possible that the transformation of morphology occurs on longer timescales than colour one (Capak et al. 2007a; Smith et al. 2005; Bamford et al. 2009; Wolf et al. 2009), as inferred also from the study of post-starburst galaxies selected in the same zCOSMOS sample (Vergani et al. 2009) or through different evolutionary paths (Skibba et al. 2008). A more comprehensive study should be performed to investigate this point, since the larger number of photometric early types compared with the morphological ones can also be due to a large fraction of dust-reddened spiral galaxies.

In COSMOS, using photometric redshifts between $z = 0.1$ and $z = 1.1$, Scoville et al. (2007a) and Capak et al. (2007a) find that, in the core of the large scale structures they identify, galaxies are characterised by earlier types, as defined by the SED and by the morphology, than in low density environments at the same redshifts, demonstrating a correlation between galaxy evolution and environment. In particular, Capak et al. (2007a) using $\sim 33,000$ galaxies, find that the rate of transformation of spiral and irregular galaxies to elliptical and lenticular ones is faster in denser regions, whereas the star formation – density relation is evolving at all densities and redshifts; thus the mechanisms of the transformation of morphology and star formation must be different.

To evaluate the uncertainties connected with this comparison on photometric and morphological types, we changed the threshold separating elliptical galaxies from late morphological types: we divided the morphological class 2.1, which should still represent bulge dominated galaxies, following the observed $B - z$: the evolutionary track of the $B - z$ colour of a galaxy Sab (Coleman et al. 1980) provides a criterion to separate quiescent and star forming galaxies in good agreement with the spectral classification, as shown in Mignoli et al. (2009). With this separation, the values of morphological M_{cross} become consistent with the photometric ones, both in the absolute values and in the trend with redshift.

Both the mechanisms, gas stripping and interactions, should be in place to explain the suppression of the star formation and the morphological transformation. Those processes act in different timescales and are characterised by different efficiencies as a function of galaxy mass and environment, but it is still difficult to draw firm conclusions, because of the caveat associated with the galaxy classification.

5.2. Comparison with mock catalogues

We used 12 mocks COSMOS mock lightcones (Kitzbichler & White 2007) based on the Millennium N-body simulation (Springel et al. 2005). The galaxy population of lightcones has then been assigned by means of semi-analytical recipes (Croton et al. 2006; De Lucia & Blaizot 2007). The final catalogues are the same described in Knobel et al. (2009), who used them to test the group finder algorithm.

In this section we used 5NN flux limited $1 + \delta$ estimate of the environment and the rest-frame colour $B - I$ to separate early

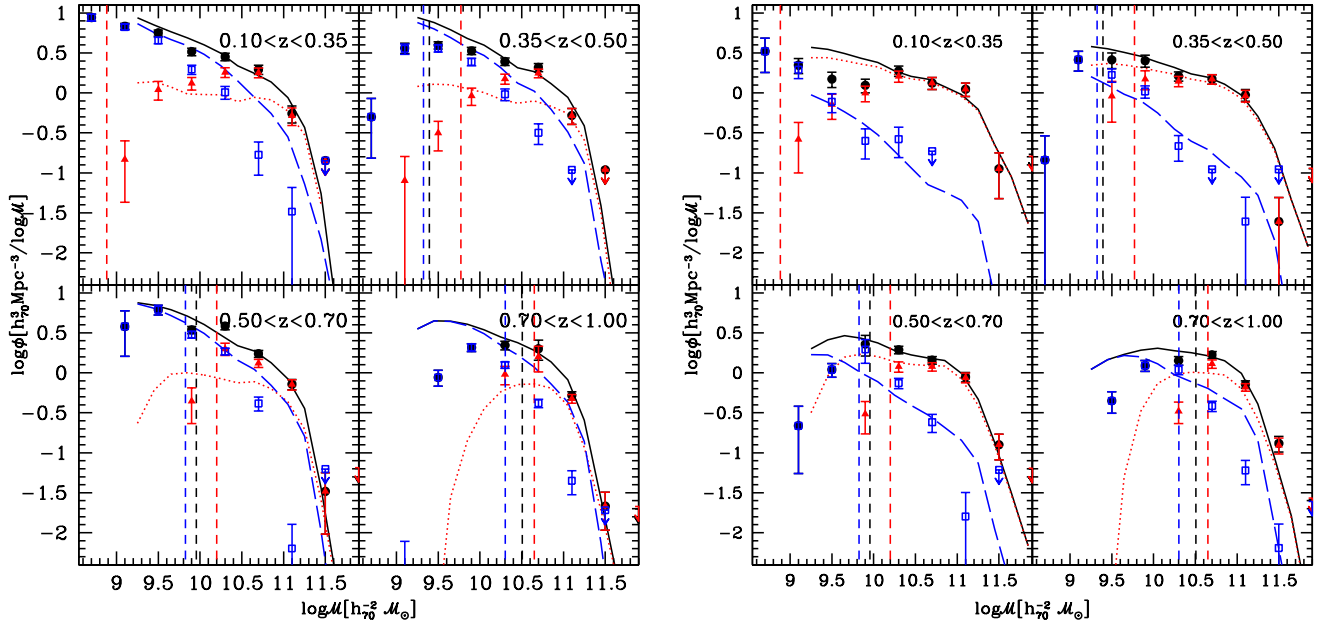


Fig. 10. Left: quartile D1 (low density environment). Right: quartile D4 (high density). Points refer to the observed quantities, lines to the GSMFs derived from the mock catalogues. Black points and solid lines: GSMFs relative to the considered density quartile, renormalised to the same integral at $\log M/M_\odot > 10.5$. Red triangles and dotted lines: galaxies with $B - I > 1.15$. Blue squares and dashed lines: galaxies with $B - I \leq 1.15$.

and late type galaxies, to be able to compare the same quantities in observations and mocks. Even though at the lowest stellar masses the mock catalogues can suffer colour incompleteness, this does not affect our analysis, since we limit our comparison to the higher masses probed in the zCOSMOS. In Fig. 9 we compare the high and low-density GSMFs in the observed sample and in the 12 averaged mock catalogues; to avoid normalisation uncertainties due to cosmic variance (Meneux et al. 2009) we decided to renormalise GSMFs, in such a way that observed and mock GSMFs of the overdense regions have the same integral at masses larger than $10^{10.5} M_\odot$ in all the redshift bins. The most evident feature of the observed GSMFs, namely the bimodality of the GSMFs in overdense regions at low redshift, is not reproduced by semi-analytical models. To explore what causes the failure of the semi-analytical models (SAMs) in reproducing observations, we separated red and blue galaxies adopting the threshold $B - I = 1.15$, that corresponds to the location of the dip of the colour bimodality, obtaining the GSMFs in Fig. 10. Considering first the low density environments, SAMs produce too many blue galaxies at intermediate and especially at high masses in all the redshift bins, and consequently also a too low density of red galaxies, in particular at $10^{10} - 10^{11} M_\odot$. This can be ascribed to an inefficient suppression of the star formation in absence of external drivers, as in the case of sparse environments. Instead, in the high density regions the most visible difference is the excess of production of low and intermediate mass red galaxies ($< 10^{10} M_\odot$) in SAMs with respect to the observed ones in the lowest redshift bin, where the probed mass range is wider. This last comparison reflect the problem of overquenching of satellites in the SAMs we used, producing too many small red galaxies: a too efficient strangulation produces an instantaneous shut down of the star formation when a galaxy enters in a halo (see Weinmann et al. 2006; Font et al. 2008; Kang & van den Bosch 2008; Kimm et al. 2009; Fontanot et al.

2009, for a description of the issue and some attempts to solve it).

6. Conclusions

We computed GSMFs in different environments and studied the relative contribution of different galaxy types and their evolution. Our main results are:

1. the bimodality seen in the global GSMF (Pozzetti et al. 2009) up to $z \sim 0.5$ is considerably enhanced in high density environments; a sum of two Schechter functions is thus required to reproduce the observed non-parametric estimates of the GSMF;
2. the bimodality is due to the different relative contribution of early and late-type galaxies in different environments, each contribution being reasonably well represented by a single Schechter function;
3. the shapes of the GSMFs of the different galaxy types and their evolution are quasi-universal, i.e., only the normalisation can be significantly different in the extreme environments we considered;
4. the evolution of the fractional contribution of different galaxy types to the environmental GSMF appears to be a function of the overdensity in which the galaxies live, consistent with an accelerated trend of downsizing in overdense regions;
5. the evolution of the crossover mass for late and early photometric type galaxies suggests a faster transition rate in overdense regions, with galaxies in low-density regions experiencing the same evolutionary path as the analogous galaxies in overdense environments with a delay of ~ 2 Gyr accumulated from $z \sim 1$ to $z \sim 0.2$;
6. the environment starts to play a significant role in the story of galaxies at $z \lesssim 1$;

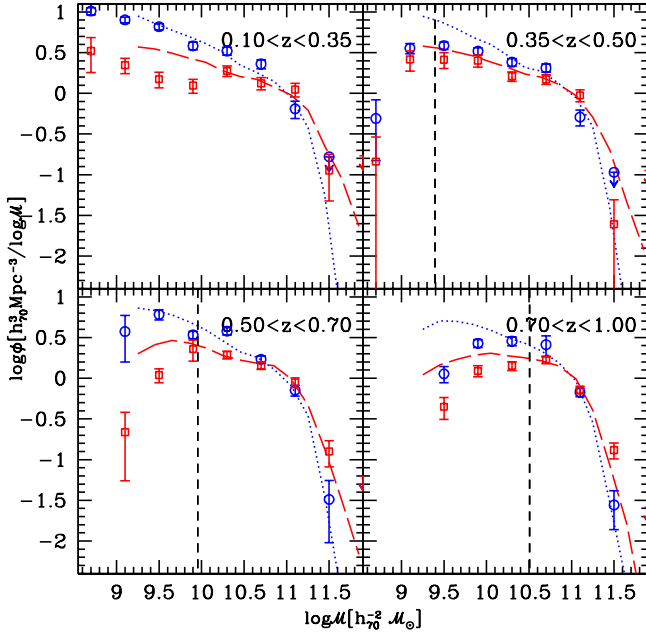


Fig. 9. GSMFs derived with $1/V_{\max}$ method in mock catalogues (D1 environment: blue dotted lines, D4: red dashed lines, both representing the average obtained from 12 mocks) compared to the observed ones (points) in D1 and D4 environments (blue circles and red squares, respectively). The functions are rescaled to arbitrary units, in order to have the same integral of the GSMFs in the overdense regions at masses larger than $10^{10.5} M_{\odot}$ in observed and mocks samples.

7. the timescales for quenching of star formation and for morphological metamorphosis are different in different environments; tentatively, the crossover mass considering morphological classification suggest that the morphological transformation is a delayed process compared to the colour change;
8. SAMs fail in different ways as a function of the environment: GSMFs computed from mock catalogues show an underestimate of the number of red massive galaxies in low density environments, probably due to an inefficient internal mechanism suppressing the star formation at relatively high masses; in high density regimes the overquenching problem of satellites in SAMs causes an excess of red galaxies at intermediate and low masses.

As a consequence of the remarkable difference in the shape of the GSMFs in under and overdense regions, we can infer that all the galaxy properties depending on mass will also depend on environment by virtue of the GSMF environmental dependence, as shown in the case of the colour-density and morphology-density relations (Cucciati et al. 2009; Tasca et al. 2009) and of the AGN fraction (Silverman et al. 2009).

The nature vs nurture debate is an inextricable problem, since the mass of a galaxy, often referred to as its nature, is a strong function of the environment. A more relevant issue is the understanding of the mechanisms producing the observed evolution of galaxies and their transition from late to early type in different environments.

Future investigations will also concern the impact of merging in different environments (de Ravel et al. 2009a; Kampczyk et al. 2009) and of the role of the dark matter halo mass function in

different environments (e.g. Abbas & Sheth 2007) in the galaxy formation efficiency.

Acknowledgements. This work was partly supported by an INAF contract PRIN/2007/1.06.10.08 and an ASI grant ASI/COFIS/WP3110 I/026/07/0

References

- Abbas, U. & Sheth, R. K. 2007, *MNRAS*, 378, 641
 Avni, Y. & Bahcall, J. N. 1980, *ApJ*, 235, 694
 Baldry, I. K., Balogh, M. L., Bower, R. G., et al. 2006, *MNRAS*, 373, 469
 Baldry, I. K., Glazebrook, K., Brinkmann, J., et al. 2004, *ApJ*, 600, 681
 Baldry, I. K., Glazebrook, K., & Driver, S. P. 2008, *MNRAS*, 388, 945
 Balogh, M. L., Baldry, I. K., Nichol, R., et al. 2004, *ApJ*, 615, L101
 Balogh, M. L., Christlein, D., Zabludoff, A. I., & Zaritsky, D. 2001, *ApJ*, 557, 117
 Bamford, S. P., Nichol, R. C., Baldry, I. K., et al. 2009, *MNRAS*, 393, 1324
 Blanton, M. R., Eisenstein, D., Hogg, D. W., Schlegel, D. J., & Brinkmann, J. 2005, *ApJ*, 629, 143
 Bolzonella, M., Miralles, J.-M., & Pelló, R. 2000, *A&A*, 363, 476
 Boselli, A. & Gavazzi, G. 2006, *PASP*, 118, 517
 Bottini, D., Garilli, B., Maccagni, D., et al. 2005, *PASP*, 117, 996
 Bruzual, G. & Charlot, S. 2003, *MNRAS*, 344, 1000
 Bundy, K., Ellis, R. S., Conselice, C. J., et al. 2006, *ApJ*, 651, 120
 Calzetti, D., Armus, L., Bohlin, R. C., et al. 2000, *ApJ*, 533, 682
 Capak, P., Abraham, R. G., Ellis, R. S., et al. 2007a, *ApJS*, 172, 284
 Capak, P., Aussel, H., Ajiki, M., et al. 2007b, *ApJS*, 172, 99
 Chabrier, G. 2003, *PASP*, 115, 763
 Charlot, S. & Bruzual, G. 2009, in preparation
 Coleman, G. D., Wu, C.-C., & Weedman, D. W. 1980, *ApJS*, 43, 393
 Cooper, M. C., Newman, J. A., Weiner, B. J., et al. 2008, *MNRAS*, 383, 1058
 Croton, D. J., Springel, V., White, S. D. M., et al. 2006, *MNRAS*, 365, 11
 Cucciati, O., Iovino, A., Kovac, K., et al. 2009, *A&A* submitted
 Cucciati, O., Iovino, A., Marinoni, C., et al. 2006, *A&A*, 458, 39
 De Lucia, G. & Blaizot, J. 2007, *MNRAS*, 375, 2
 de Ravel, L., Kampczyk, P., & zCOSMOS collaboration. 2009a, *A&A* to be submitted
 de Ravel, L., Le Fèvre, O., Tresse, L., et al. 2009b, *A&A*, 498, 379
 Dressler, A. 1980, *ApJ*, 236, 351
 Elbaz, D., Daddi, E., Le Borgne, D., et al. 2007, *A&A*, 468, 33
 Feldmann, R., Carollo, C. M., Porciani, C., et al. 2006, *MNRAS*, 372, 565
 Feldmann, R., Carollo, C. M., Porciani, C., Lilly, S. J., & Oesch, P. 2008, *ArXiv e-prints*, 0801.3275
 Finoguenov, A. & COSMOS collaboration. 2009, *ApJ* in preparation
 Finoguenov, A., Guzzo, L., Hasinger, G., et al. 2007, *ApJS*, 172, 182
 Font, A. S., Bower, R. G., McCarthy, I. G., et al. 2008, *MNRAS*, 389, 1619
 Fontana, A., Pozzetti, L., Donnarumma, I., et al. 2004, *A&A*, 424, 23
 Fontanot, F., De Lucia, G., Monaco, P., Somerville, R. S., & Santini, P. 2009, *ArXiv e-prints*, 0901.1130
 Garilli, B. 2009, in preparation
 Gehrels, N. 1986, *ApJ*, 303, 336
 Hogg, D. W., Blanton, M. R., Eisenstein, D. J., et al. 2003, *ApJ*, 585, L5
 Ilbert, O., Arnouts, S., McCracken, H. J., et al. 2006, *A&A*, 457, 841
 Ilbert, O., Capak, P., Salvato, M., et al. 2009a, *ApJ*, 690, 1236
 Ilbert, O., Salvato, M., Le Floc'h, E., et al. 2009b, *ApJ* submitted
 Ilbert, O., Tresse, L., Arnouts, S., et al. 2004, *MNRAS*, 351, 541
 Ilbert, O., Tresse, L., Zucca, E., et al. 2005, *A&A*, 439, 863
 Iovino, A., Cucciati, O., Scodreggio, M., et al. 2009, *A&A* submitted
 Jenkins, L. P., Hornschemeier, A. E., Mobasher, B., Alexander, D. M., & Bauer, F. E. 2007, *ApJ*, 666, 846
 Kampczyk, P. & zCOSMOS collaboration. 2009, *ApJ* to be submitted
 Kang, X. & van den Bosch, F. C. 2008, *ApJ*, 676, L101
 Kauffmann, G., Heckman, T. M., Tremonti, C., et al. 2003, *MNRAS*, 346, 1055
 Kauffmann, G., White, S. D. M., Heckman, T. M., et al. 2004, *MNRAS*, 353, 713
 Kimm, T., Somerville, R. S., Yi, S. K., et al. 2009, *MNRAS*, 394, 1131
 Kinney, A. L., Calzetti, D., Bohlin, R. C., et al. 1996, *ApJ*, 467, 38
 Kitzbichler, M. G. & White, S. D. M. 2007, *MNRAS*, 376, 2
 Knobel, C., Lilly, S. J., Iovino, A., et al. 2009, *ApJ*, 697, 1842
 Koekemoer, A. M., Aussel, H., Calzetti, D., et al. 2007, *ApJS*, 172, 196
 Kovač, K., Lilly, S. J., Cucciati, O., et al. 2009, *ApJ* submitted
 Kovač, K. & zCOSMOS collaboration. 2009, *ApJ* to be submitted
 Kroupa, P. 2001, *MNRAS*, 322, 231
 Lee, J. & Li, C. 2008, *ArXiv e-prints*, 0803.1759
 Lilly, S., Le Brun, V., Maier, C., et al. 2009, *ApJ* to be submitted
 Lilly, S. J., Le Fèvre, O., Renzini, A., et al. 2007, *ApJS*, 172, 70
 Lin, L., Koo, D. C., Weiner, B. J., et al. 2007, *ApJ*, 660, L51

- Maier, C., Lilly, S. J., Zamorani, G., et al. 2009, *ApJ*, 694, 1099
- Maraston, C. 2005, *MNRAS*, 362, 799
- Maraston, C., Daddi, E., Renzini, A., et al. 2006, *ApJ*, 652, 85
- Marchesini, D., van Dokkum, P. G., Forster Schreiber, N. M., et al. 2008, *ArXiv e-prints*, 0811.1773
- Marigo, P. & Girardi, L. 2007, *A&A*, 469, 239
- Mateus, A., Jimenez, R., & Gaztañaga, E. 2008, *ApJ*, 684, L61
- Mateus, A., Sodré, L., Cid Fernandes, R., & Stasińska, G. 2007, *MNRAS*, 374, 1457
- McCracken, H. J., Capak, P., Salvato, M., et al. 2009, *A&A* to be submitted
- Meneux, B., Guzzo, L., de la Torre, S., et al. 2009, *ArXiv e-prints*, 0906.1807
- Mignoli, M., Zamorani, G., Scoddeggio, M., et al. 2009, *A&A*, 493, 39
- Panther, B., Heavens, A. F., & Jimenez, R. 2004, *MNRAS*, 355, 764
- Popesso, P., Biviano, A., Böhringer, H., & Romaniello, M. 2007, *A&A*, 464, 451
- Pozzetti, L., Bolzonella, M., Lamareille, F., et al. 2007, *A&A*, 474, 443
- Pozzetti, L., Bolzonella, M., Zucca, E., et al. 2009, *A&A* to be submitted
- Salpeter, E. E. 1955, *ApJ*, 121, 161
- Sargent, M. T., Carollo, C. M., Lilly, S. J., et al. 2007, *ApJS*, 172, 434
- Scarlata, C., Carollo, C. M., Lilly, S., et al. 2007, *ApJS*, 172, 406
- Schechter, P. 1976, *ApJ*, 203, 297
- Scoddeggio, M., Franzetti, P., Garilli, B., et al. 2005, *PASP*, 117, 1284
- Scoddeggio, M., Vergani, D., Cucciati, O., et al. 2009, *ArXiv e-prints*, 0903.0271
- Scoville, N., Aussel, H., Benson, A., et al. 2007a, *ApJS*, 172, 150
- Scoville, N., Aussel, H., Brusa, M., et al. 2007b, *ApJS*, 172, 1
- Silverman, J. D., Kovač, K., Knobel, C., et al. 2009, *ApJ*, 695, 171
- Skibba, R. A., Bamford, S. P., Nichol, R. C., et al. 2008, *ArXiv e-prints*, 0811.3970
- Smith, G. P., Treu, T., Ellis, R. S., Moran, S. M., & Dressler, A. 2005, *ApJ*, 620, 78
- Spaenhauer, A. M. 1978, *A&A*, 65, 313
- Springel, V., White, S. D. M., Jenkins, A., et al. 2005, *Nature*, 435, 629
- Tanaka, M., Goto, T., Okamura, S., Shimasaku, K., & Brinkmann, J. 2004, *AJ*, 128, 2677
- Tasca, L. A. M., Kneib, J. P., Iovino, A., et al. 2009, *ArXiv e-prints*, 0906.4556
- Treu, T., Ellis, R. S., Kneib, J.-P., et al. 2003, *ApJ*, 591, 53
- van den Bosch, F. C., Pasquali, A., Yang, X., et al. 2008, *ArXiv e-prints*, 0805.0002
- Vergani, D. & zCOSMOS collaboration. 2009, *A&A* to be submitted
- Weinmann, S. M., van den Bosch, F. C., Yang, X., et al. 2006, *MNRAS*, 372, 1161
- Wolf, C., Aragón-Salamanca, A., Balogh, M., et al. 2009, *MNRAS*, 393, 1302
- Zucca, E., Bardelli, S., Bolzonella, M., et al. 2009, *A&A* submitted
- Zucca, E., Ilbert, O., Bardelli, S., et al. 2006, *A&A*, 455, 879
- Zucca, E., Pozzetti, L., & Zamorani, G. 1994, *MNRAS*, 269, 953
- Zucca, E., Zamorani, G., Vettolani, G., et al. 1997, *A&A*, 326, 477
- ¹⁶ Centre de Physique Theorique, Marseille, France
- ¹⁷ Institut d'Astrophysique de Paris, UMR 7095 CNRS, Université Pierre et Marie Curie, 98 bis Boulevard Arago, F-75014 Paris, France
- ¹⁸ Argelander-Institut für Astronomie, Auf dem Hügel 71, D-53121 Bonn, Germany
- ¹⁹ INAF, Osservatorio Astronomico di Roma, via di Frascati 33, I-00040 Monteporzio Catone, Italy
- ²⁰ AIM Unité Mixte de Recherche CEA CNRS, Université Paris VII UMR n158, Paris, France
- ²¹ California Institute of Technology, MC 105-24, 1200 East California Boulevard, Pasadena, CA 91125, USA
- ²² Institute for Astronomy, University of Hawaii, 2680 Woodlawn Drive, Honolulu, HI, 96822
- ²³ Spitzer Science Center, Pasadena, CA, USA
- ²⁴ Research Center for Space and Cosmic Evolution, Ehime University, Bunkyo-cho, Matsuyama 790-8577, Japan
- ²⁵ Large Binocular Telescope Observatory, University of Arizona, 933 N. Cherry Ave., Tucson, AZ 85721-0065, USA

¹ INAF - OA Bologna, via Ranzani 1, I-40127 Bologna - Italy

² Institute of Astronomy, Swiss Federal Institute of Technology (ETH Hönggerberg), CH-8093, Zürich, Switzerland

³ Laboratoire d'Astrophysique de Marseille, Université d'Aix-Marseille, CNRS, 38 rue Frederic Joliot-Curie, F-13388 Marseille Cedex 13, France

⁴ INAF - Osservatorio Astronomico di Brera, via Brera 28, I-20121 Milano, Italy

⁵ INAF - IASF Milano, via Bassini 15, I-20133 Milano, Italy

⁶ Laboratoire d'Astrophysique de Toulouse-Tarbes, Université de Toulouse, CNRS, 14 avenue Edouard Belin, F-31400 Toulouse, France

⁷ INAF - Osservatorio Astronomico di Torino, I-10025 Pino Torinese, Italy

⁸ European Southern Observatory, Karl-Schwarzschild-Strasse 2, Garching, D-85748, Germany

⁹ Dipartimento di Astronomia, Università di Padova, Padova, Italy

¹⁰ Max-Planck-Institut für extraterrestrische Physik, D-84571 Garching, Germany

¹¹ Dipartimento di Astronomia, Università di Bologna, via Ranzani 1, I-40127, Bologna, Italy

¹² Instituto de Astrofísica de Andalucía, CSIC, Apdo. 3004, 18080, Granada, Spain

¹³ University of Massachusetts, Amherst, USA

¹⁴ LBNL & BCCP, University of California, Berkeley, CA 94720, USA

¹⁵ Space Telescope Science Institute, 3700 San Martin Drive, Baltimore, MD 21218, USA